State-Selective Quantum Interference Observed in the Recombination of Highly Charged $Hg^{75+\cdots 78+}$ Mercury Ions in an Electron Beam Ion Trap

A. J. González Martínez, J. R. Crespo López-Urrutia, J. Braun, G. Brenner, H. Bruhns, A. Lapierre, V. Mironov, R. Soria Orts, H. Tawara, M. Trinczek, and J. Ullrich
Max-Planck Institute for Nuclear Physics, D-69117 Heidelberg, Germany

J. H. Scofield
Lawrence Livermore National Laboratory, Livermore, California 94550, USA
(Received 16 November 2004; published 23 May 2005)

We present experimental data on the state-selective quantum interference between different pathways of photorecombination, namely, radiative and dielectronic recombination, in the KLL resonances of highly charged mercury ions. The interference, observed for well resolved electronic states in the Heidelberg electron beam ion trap, manifests itself in the asymmetry of line shapes, characterized by "Fano factors," which have been determined with unprecedented precision, as well as their excitation energies, for several strong dielectronic resonances.

DOI: 10.1103/PhysRevLett.94.203201 PACS numbers: 34.80.Kw, 32.80.Hd, 52.25.Os

One of the most striking consequences of the wave-matter dualism is the appearance of quantum interference phenomena [1]. These effects are ubiquitous in essentially all fields: from lasers [2] to solid-state physics [3], magnetism [4], electron collisions [5], and nanotechnology [6], to name but a few. As a result, asymmetric resonance line profiles are observed whenever resonant and nonresonant pathways interfere.

Indeed, more than 40 years ago, Fano [7,8] predicted the interference between transition amplitudes leading directly into the ionization continuum (DPI in Fig. 1) and those indirectly proceeding via a discrete autoionizing intermediate resonant state (IPI in Fig. 1), resulting in asymmetric line shapes for the energy-dependent photoionization spectra around the resonance. Meanwhile, such interferences, sometimes with far-reaching consequences and remarkable changes in total cross sections, have been widely explored in experiments (for a review see, e.g., [9]). Evidence for the interference in the time-reversed process, namely, the recombination of a free electron with an ion (Li-like in Fig. 1), though being of paramount importance for terrestrial as well as for astrophysical plasmas, has only been observed in one single experiment using a mixture of various charge states of uranium ions in the LLNL SuperEBIT [10].

Although the two amplitudes, the direct recombination under emission of a photon, or "radiative" recombination (RR), and the indirect process, called "dielectronic" recombination (DR) where the excited intermediate state is stabilized via photon emission at identical energy, can in principle interfere, Fano profiles can hardly be observed in an experiment. This is due to the fact that for low- and intermediate-Z ions (Z, nuclear charge) RR is a weak process with cross sections on the order of 10^{-22} cm^2 [11], whereas DR is strong (10^{-17} cm^2), resulting in a large difference in the magnitude of the amplitudes, thus making interference effects negligible. For highly charged ions (HCI), instead, stronger interference effects are expected, since the two amplitudes become comparable in magnitude due to the fact that the cross section for RR scales with Z^2 whereas the one for DR is roughly independent of Z.

In this Letter, we report on the observation of distinct Fano profiles in the photorecombination spectra around DR resonances for highly charged He- to B-like mercury ions $Hg^{75+\cdots 78+}$. Detecting the emitted photons, single resonances for well defined ion charge states have been isolated for the first time and asymmetry parameters, so-called Fano factors, have been extracted at an unprecedented 6% accuracy level for the strongest transitions. Apart from the results for Be-like ions, our data are found to be in good agreement with the predictions of fully relativistic multiconfiguration Dirac-Fock (MCDF) calculations, including quantum electrodynamic (QED) contributions on a typical level of 162 eV (one 1s electron) and nuclear size effects about half as large, both with an

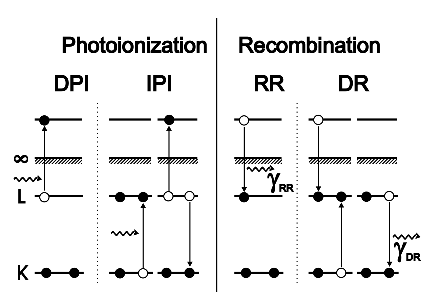

FIG. 1. Two different pathways for the ionization process are shown on the left side of the figure corresponding to the direct photoionization (DPI) and the indirect photoionization (IPI). The picture on the right side illustrates the time-reversed RR and DR processes.

absolute accuracy of ± 14 eV, just matching our experimentally achieved accuracy at electron energies around 50 keV.

In one of the few existing calculations analyzing quantum interference between RR and DR, Badnell and Pindzola [12] predicted a large increase of the effect if KLL resonances for HCIs are considered [13], and also Zimmerman treated them [14]. Here a free electron is captured into the $n = 2$ (L) shell while an $n = 1$ (K) electron is lifted to $n = 2$. For those KLL resonances to be observed requires not only the production of highly charged ions in sufficient numbers, which can only be achieved by four machines worldwide, the GSI ESR storage ring and the EBITs in Livermore, Heidelberg [15], and Tokyo [16], but, moreover, demands high relative energies between electrons and HCIs, which have just become accessible in storage rings [17,18].

Even for lighter ions, Jacobs, Cooper, and Haan [19] predicted clearly discernable interference patterns by treating both photorecombination processes in a unified description, taking the interference term explicitly into account in their calculation of the total ion-electron loss cross section. In storage rings, a small experimental evidence for an asymmetry in the line shape of the recombination rate due to DR-RR interference was reported by Schippers [20] at low energies in Ar-like Sc^{3+}.

The EBIT operated with an electron beam of 160 mA compressed to a diameter of less than 0.1 mm with an 8 T magnetic field. Its negative space-charge potential confines the ions radially. Several drift tubes are used to trap the ions longitudinally. In this way, an ion cloud of 40 mm length and roughly 0.2 mm diameter is produced. Ionization takes place inside this trap volume through successive collisions with the electron beam. A variable photon energy in the photoionization process corresponds to a variable electron energy in the time-reversed photorecombination experiment. The electron beam energy was slowly scanned (37 V/s) in a sawtooth pattern across the KLL resonances (45–53 keV) in order to maintain the electron impact ionization in equilibrium with the recombination at each beam energy (steady state). The beam energy was measured with a high-accuracy voltage divider. Although the space-charge correction applied delivered the energies of the main He-like resonances to within ± 5 eV, in Table I we have referenced the energy scale to the theoretical value (this work, MCDF) of the first He-like resonance.

A high-purity Ge detector mounted at 90° relative to the electron beam axis was used for x-ray detection. This detector was calibrated at regular intervals to account for slow gain drifts in the data acquisition system. Single event acquisition is triggered by the arrival of an x-ray photon (γ_{DR}, γ_{RR}, or bremsstrahlung). Both the photon and electron beam energies are simultaneously recorded. After a data acquisition time of around 100 hours, a two-dimensional map (photon vs electron energy) of the photorecombination rate was obtained (see Fig. 2). Here, two diagonal bands due to RR are clearly visible: the upper band represents RR into states $n = 2$ with the total angular momentum $J = 1/2$, and the lower and broader band into those with $J = 3/2$. The x-ray energy difference between the two bands is approximately 2 keV. A stronger yield of x rays appears concentrated on five clusters of horizontally aligned bright spots, due to DR resonances of mercury ions with open L shell. In accordance to the nomenclature introduced in Ref. [10] they are labeled $KL_{12}L_{12}$ (left one), $KL_{12}L_3$ (two central clusters), and KL_3L_3 (two right clusters). Four of the clusters strongly overlap with the RR bands. For a He-like initial state they represent the DR into the final states $KL_{J=1/2}L_{J=1/2}$ ($1s2s^2$, $1s2s2p_{1/2}$, $1s2p_{1/2}2p_{1/2}$), $KL_{J=1/2}L_{J=3/2}$ ($1s2s2p_{3/2}$, $1s2p_{1/2}2p_{3/2}$), and $KL_{J=3/2}L_{J=3/2}$ ($1s2p_{3/2}2p_{3/2}$), respectively. These denominations are used for other charge states in an analogous way.

By projecting specific regions of this plot either onto the electron beam or onto the x-ray energy axis, detailed information can be extracted (see Figs. 3 and 4). The broadbands mentioned above can be sliced into narrower cuts which allow us to study the interference for specific charge states, because of the fact that the photon energies on the upper and the bottom slices of each RR band

TABLE I. Theoretical (MCDF) and measured Fano factors (q), and measured energies for the strongest DR resonances. For the He_1 fit a symmetric profile was used. The fit to B_3 resulted in an almost symmetric profile.

Label	Excited state	J	q_{theo}	q_{meas}	E_k (keV)
He_1	$1s2s^2$	1/2	−140	sym.	46.358
Li_1	$1s2s^22p_{1/2}$	1	−12.2	−14.2(2.2)	46.686(5)
Be_1	$1s2s^2(2p_{1/2})^2$	1/2	−12	−9.3(0.9)	47.135(5)
Be_3	$(1s2s^22p_{1/2})_02p_{3/2}$	3/2	7.3	6.7(0.6)	49.349(6)
Be_4	$(1s2s^22p_{1/2})_12p_{3/2}$	5/2	13	18.2(6.6)	49.265(17)
Be_5	$1s2s^2(2p_{3/2})^2{}_2$	5/2	16.3	11.1(2.0)	51.433(6)
B_1	$1s2s^2(2p_{1/2})^22p_{3/2}$	1	5.2	5.1(0.3)	49.557(4)
B_2	$1s2s^2(2p_{1/2})^22p_{3/2}$	2	9	10(1)	49.499(4)
B_3	$1s2s^2(2p_{1/2})^22p_{3/2}$	1	−441	sym.	49.552(7)

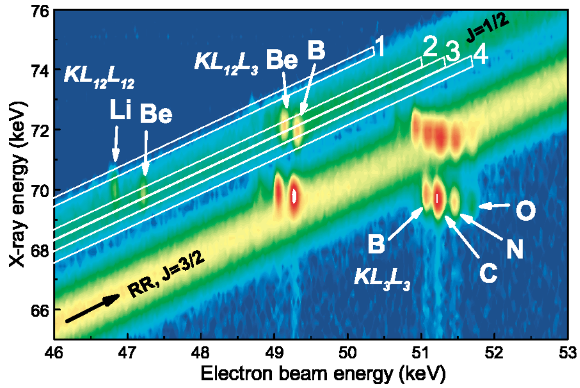

FIG. 2 (color). Logarithmic 2D contour plot of the KLL resonances for highly charged mercury ions. The diagonal bands correspond to RR processes into $J = 1/2$ (upper) and $J = 3/2$ (lower). DR processes are visible as single bright spots. The areas 1 thru 4 (outlined in white) in the upper RR band for $J = 1/2$ indicate thin cuts, whose projection onto the electron beam axis is shown in Figs. 3 and 4.

correspond to different ion charge states. For example, the upper slice of the RR $J = 1/2$ band shows the He-like ion charge state along with a fraction of Li-like ions [Fig. 3(a), cut 1]. In contrast, in a lower slice (Fig. 2, cut 2) a strong Be-like peak is observed with a very weak contribution from a Li-like resonance [Fig. 3(b), cut 2]. The lowest slice of this band showed almost an exclusive population of B-like ions as shown in Fig. 4(b), cut 4. Other cuts parallel to the $J = 3/2$ band but shifted to lower x-ray energies pass through a set of DR resonances which do not overlap with the RR process, since the photon is emitted by a transition from a $J = 1/2$ level, whereas the foregoing recombination filled a $J = 3/2$ vacancy. Thus, no quantum interference is expected to occur here, and accordingly the observed line profiles are symmetrical.

In order to fit the asymmetric experimental data, we used for each single electronic state a Fano profile function in the way described by Schippers [20],

$$F(E) = \frac{A}{q^2\Gamma_d}\frac{2}{\pi}\left[\frac{(\epsilon + q)^2}{\epsilon^2 + 1} - 1\right], \qquad \epsilon = \frac{2(E_e - E_k)}{\Gamma_d} \tag{1}$$

where q is the so-called Fano factor which gives information on the degree of asymmetry, A defines the peak area, and Γ_d is the natural width of the resonance. E_e and E_k are the incoming electron and the resonance energy, respectively. It is noted that for large values of q the function converges to a Lorentzian, while for small values a stronger asymmetry is expected.

To account for the electron energy spread, the theoretical Fano profile is convoluted with a normalized Gaussian distribution. The convolution results in a function which contains the real and imaginary parts of the so-called complex error function. These terms were obtained using an algorithm given by Humlicek [21], who treated an analogous situation. The analysis showed an experimental width of about 60 eV at 50 keV electron beam energy, corresponding to a relative resolution $\Delta E/E \approx 1/1000$. In the pioneering work of Knapp *et al.*, all resonances corresponding to an individual charge state were averaged according to their DR strengths, and a mean q was determined for that given ion. In contrast, in the present work, the Fano factors of well resolved individual resonances were extracted (see Table I). For the fitting procedure, the natural width Γ_d is the only parameter taken from theory. A few resonances of negligible strength, such as

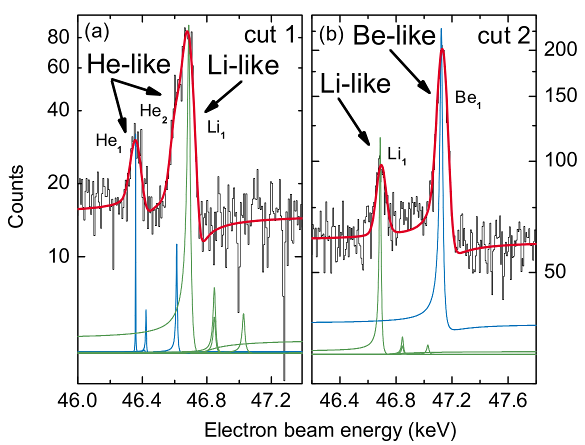

FIG. 3 (color). Experimental (black curve) and fitted (red curve) data for two different slices of the RR $n = 2$, $J = 1/2$ in the $KL_{12}L_{12}$ region whose analysis shows negative Fano factors in comparison with a normalized nonconvoluted theoretical cross section (blue and green curves). Left: Projection of the upper slice where He- and Li-like ions are observed. Right: Projection of an intermediate region showing Be- and Li-like resonances.

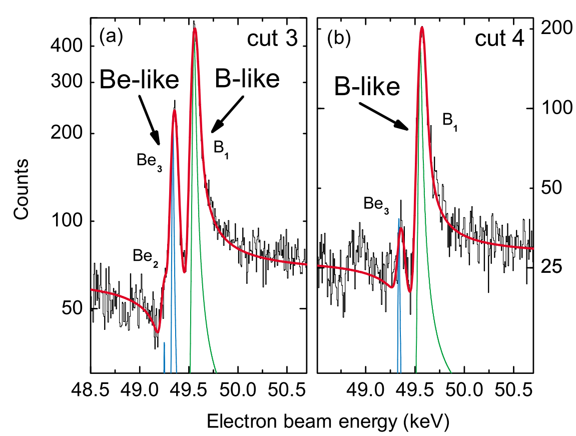

FIG. 4 (color). In comparison with the He- and Li-like resonances in the $KL_{12}L_{12}$ region (see Fig. 3) the $KL_{12}L_3$ Be- and B-like ones show opposite, i.e., positive Fano factors. The two cuts displayed here exemplify the method used to resolve resonances from specific charge states. In these pictures are also shown the normalized nonconvoluted theoretical cross section (blue and green curves).

those shown with their theoretical normalized strengths, widths, and positions in Fig. 3 were not taken into account for the fitting procedure.

The fit quality was evaluated with the χ^2 over degrees-of-freedom (DOF) method. In general, the interference becomes obvious when the χ^2/DOF parameter of the different fits and their corresponding residuals are considered. For instance, we obtained from the Lorentzian fit a χ^2/DOF of 3.8, whereas a Fano fit results in a much better χ^2/DOF of 1.3 for the $KL_{12}L_3$ region in the $J = 1/2$ band. Other cuts between RR into $n = 2$ ($J = 3/2$) and RR into $n = 3$ containing two-photon transitions, showed symmetric profiles, as expected. For some of the He- and B-like states, the calculated Fano factors are very large, resulting in nearly completely symmetric peak profiles, which could be observed. Thus, the asymmetry only appears in the excitation of those states where it was predicted. This confirms that the observed asymmetry is not an artifact produced by our data acquisition system or by the data analysis.

Theoretical DR cross sections have been calculated using a relativistic MCDF method similar to those carried out for uranium ions [10] by Scofield [22]. The relativistic MCDF method treats the relativistic electron radiative recombination onto an ion followed from the S-matrix development of relativistic quantum electrodynamics. A multipole expansion is used for the emitted photon states, but only the electric dipole and quadrupole contributions are significant. Continuum states are implemented into the code. The DR process is introduced by including the coupling between the continuum states and the doubly excited states. Admixtures of the doubly excited states are added to the continuum state to the lowest order. The interaction between the continuum states and bound states in the code includes both the Coulomb and retarded Breit interactions. The matrix element for the emission includes the purely continuum part and sums over the excited bound states. The asymmetric terms come from the cross terms when the matrix element is squared in calculating the cross section.

Indeed, the theoretical differential DR cross sections including the natural widths have shown strong asymmetrical interference profiles. The calculated natural widths can be in the order of 10 to 35 eV for Be- and B-like ions. The electron beam energy spread (approximately 60 eV) is comparable with the natural widths. Therefore, the asymmetry tends to become somewhat weaker when the cross sections are convoluted with this experimental resolution. As clearly seen in Table I, the observed and calculated asymmetry Fano factors, including their signs, are in good agreement with each other for all the charge states and different configurations.

In conclusion, we have demonstrated and studied experimentally the quantum interference between dielectronic and radiative recombination processes for the KLL resonances in highly charged ions. The Fano factors for several well resolved resonances has been determined with a relative error of only 6%. The results show a good agreement with theoretical predictions obtained with the MCDF method. However, small discrepancies between theory and experiment are noticeable for the Be-like systems. It should also be pointed out that with our present technique absolute excitation energies in the range of 50 keV can be determined with an experimental uncertainly as small as ± 14 eV. Their detailed analysis will be reported in a forthcoming Letter. The good overall agreement indicates that the transition amplitudes for the electron-electron and electron-photon interactions responsible for the different pathways can be predicted at a level of 10% by the current theoretical methods.

We acknowledge fruitful conversations with A. Artemyev and I. Tupitsyn during the preparation of this manuscript. The work at the University of California Lawrence Livermore National Laboratory was performed under the auspices of the U.S. Department of Energy under Contract No. W-7405-Eng-48.

[1] R. P. Feynman, R. B. Leighton, and M. Sands, *The Feynman Lectures on Physics*, Quantum Mechanics Vol. 3 (Addison-Wesley, New York, 1965).
[2] A. S. Zibrov *et al.*, Phys. Rev. Lett. **75**, 1499 (1995).
[3] J. Faist, F. Capasso, C. Sirtori, K. W. West, and L. N. Pfeiffer, Nature (London) **390**, 589 (1997).
[4] V. Madhavan, W. Chen, T. Jamneala, M. F. Crommie, and N. S. Wingreen, Science **280**, 567 (1998).
[5] R. C. Liu, B. Odom, Y. Yamamoto, and S. Tarucha, Nature (London) **391**, 263 (1998).
[6] R. K. Kawakami *et al.*, Phys. Rev. Lett. **80**, 1754 (1998).
[7] U. Fano, Phys. Rev. **124**, 1866 (1961).
[8] U. Fano and J. W. Cooper, Phys. Rev. **137**, A1364 (1965).
[9] U. Eichmann, T. F. Gallagher, and R. M. Konik, Phys. Rev. Lett. **90**, 233004 (2003).
[10] D. A. Knapp, P. Beiersdorfer, M. H. Chen, J. H. Scofield, and D. Schneider, Phys. Rev. Lett. **74**, 54 (1995).
[11] *Atomic Physics with Heavy Ions*, edited by H. F. Beyer and V. P. Shevelko (Springer, Heidelberg, 2002).
[12] N. R. Badnell and M. S. Pindzola, Phys. Rev. A **45**, 2820 (1992).
[13] M. S. Pindzola, N. R. Badnell, and D. C. Griffin, Phys. Rev. A **46**, 5725 (1992).
[14] M. Zimmermann, N. Grün, and W. Scheid, J. Phys. B **30**, 5259 (1997).
[15] J. R. Crespo López-Urrutia, A. Dorn, R. Moshammer, and J. Ullrich, Phys. Scr. **T80**, 502 (1999).
[16] F. J. Currell *et al.*, J. Phys. Soc. Jpn. **65**, 3186 (1996).
[17] C. Brandau *et al.*, GSI Scientific Report No. GSI 2003-1, p. 91f.
[18] A. Müller (private communication).
[19] V. L. Jacobs, J. Cooper, and S. L. Haan, Phys. Rev. A **36**, 1093 (1987).
[20] S. Schippers *et al.*, Phys. Rev. A **65**, 042723 (2002).
[21] J. Humlicek, J. Quant. Spectrosc. Radiat. Transfer **21**, 309 (1979).
[22] J. H. Scofield, Phys. Rev. A **40**, 3054 (1989).